molecules

MDPI

Article

Anti-Neuroinflammatory Components from *Clausena lenis* Drake

Si-Si Zhu, Yi-Fan Zhang, Meng Ding, Ke-Wu Zeng, Peng-Fei Tu and Yong Jiang *

State Key Laboratory of Natural and Biomimetic Drugs, School of Pharmaceutical Sciences, Peking University, No. 38 Xueyuan Road, Haidian District, Beijing 100191, China; zsszmh@163.com (S.-S.Z.); yifan9986@163.com (Y.-F.Z.); stillmedingmeng@163.com (M.D.); zkw@bjmu.edu.cn (K.-W.Z.); pengfeitu@bjmu.edu.cn (P.-F.T.)
* Correspondence: yongjiang@bjmu.edu.cn

Abstract: *Clausena lenis* Drake (*C. lenis*) is a folk medicinal herb to treat influenza, colds, bronchitis, and malaria. The 95% and 50% ethanol extract of *C. lenis* showed significant nitric oxide (NO) inhibition activity in BV-2 microglial cells stimulated by lipopolysaccharide (LPS). Bio-guided isolation of the active extract afforded five new compounds, including a chlorine-containing furoquinoline racemate, (±)-claulenine A (**1**), an amide alkaloid, claulenine B (**2**), a prenylated coumarin, claulenin A (**3**), a furocoumarin glucoside, clauleside A (**4**), and a multi-prenylated *p*-hydroxybenzaldehyde, claulenin B (**5**), along with 33 known ones. Their structures were determined via spectroscopic methods, and the absolute configurations of new compounds were assigned via the electronic circular dichroism (ECD) calculations and single-crystal X-ray diffraction analysis. Compounds **2**, **23**, **27**, **28**, **33**, and **34** showed potent anti-neuroinflammatory effects on LPS-induced NO production in BV-2 microglial cells, with IC_{50} values in the range of 17.6–40.9 μM. The possible mechanism was deduced to interact with iNOS through molecular docking.

Keywords: *Clausena lenis* Drake; alkaloid; coumarin; anti-neuroinflammation; BV-2 cells

Citation: Zhu, S.-S.; Zhang, Y.-F.; Ding, M.; Zeng, K.-W.; Tu, P.-F.; Jiang, Y. Anti-Neuroinflammatory Components from *Clausena lenis* Drake. *Molecules* **2022**, *27*, 1971. https://doi.org/10.3390/molecules27061971

Academic Editor: Xinghai Liu

Received: 15 February 2022
Accepted: 16 March 2022
Published: 18 March 2022

1. Introduction

Neuroinflammation generally refers to an inflammatory response in the brain or spinal cord and has a pivotal role in the pathogenesis of neurodegenerative diseases, such as Alzheimer's disease (AD) [1] and Parkinson's disease (PD) [2,3]. This inflammation is mediated by cytokines, chemokines, reactive oxygen species, and secondary messengers produced by resident central glial cells (microglia and astrocytes), endothelial cells, and immune cells of peripheral origin [4]. Among them, microglia, as innate immune cells of the central nervous system, are major participants in neuroinflammation [1] and have various neuroimmunological functions in the central nervous system under normal and pathological conditions [5].

Phytochemicals, as the main components of natural products, have a variety of pharmacological effects, including anti-inflammation, neuroprotection, anti-cancer, and metabolism regulation [6–9]. In recent years, some compounds derived from *Clausena* species have been revealed to present potential anti-neuroinflammatory activities by inhibiting the nitric oxide (NO) production in lipopolysaccharide (LPS)-induced BV-2 microglial cells [10–12].

Clausena lenis Drake (*C. lenis*) belongs to the genus *Clausena* of Rutaceae family, distributed mainly in the Hainan, southern Guangxi, and Yunnan provinces of China [13]. It has been used as a folk medicine for the treatment of influenza, colds, bronchitis, and malaria. Alkaloids and coumarins are preliminarily verified to be its main constituents [14–19]. During our search for anti-neuroinflammatory components from *Clausena* and its closely related *Murraya* species [20–22], the 95% and 50% ethanol extract of *C. lenis* showed significant NO inhibition activity in BV-2 microglial cells stimulated by LPS with 73.5% inhibition rate at 80 ug/mL. To trace the potential anti-neuroinflammatory compounds, the ethanol extract of *C. lenis* was chemically investigated to afford 38 compounds, including five new compounds, namely (±)-claulenine A (**1**), claulenine B (**2**), claulenin A (**3**), clauleside A (**4**), and claulenin B

(**5**) (Figure 1). (±)-Claulenine A (**1**) is a racemate of furoquinoline containing chlorine, which is rare in phytochemicals. Herein, the isolation and structure elucidation of the new compounds and the inhibitory effects on LPS-induced NO of the isolates were described. Moreover, the interactions between the bioactive compounds and iNOS via molecular docking were also reported.

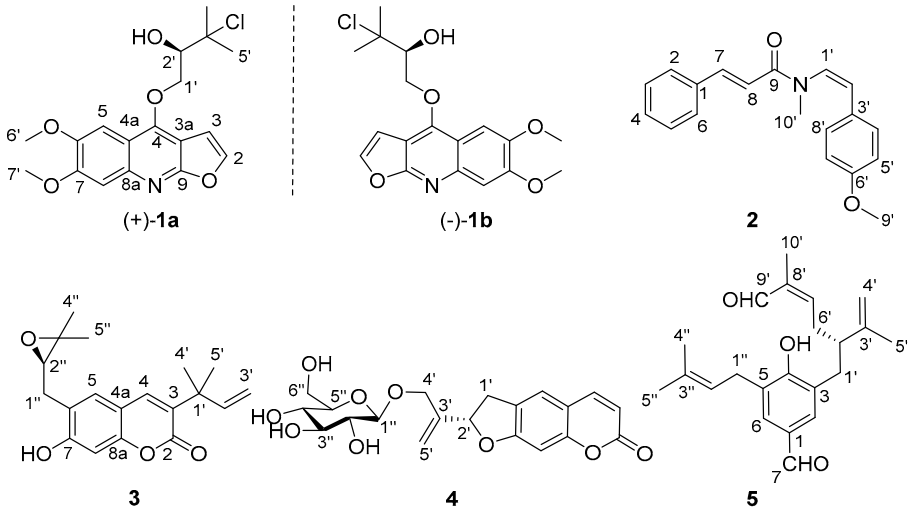

Figure 1. Chemical structures of compounds **1**−**5**.

2. Results

2.1. Structural Elucidation

(±)-Claulenine A (**1**) was obtained as a white solid, $[\alpha]_D^{25}$ 0 (*c* 0.12, MeOH). The HR-ESI-MS data indicated the presence of one chlorine in the molecule from the relative abundance (~1/3) of the isotope peaks observed at *m*/*z* 366.1101 and 368.1077, corresponding to a molecular formula of $C_{18}H_{20}NO_5Cl$ (calcd for $C_{18}H_{21}NO_5Cl$, 366.1108; mass error −1.9 ppm), with nine degrees of unsaturation. Analysis of the ^{1}H-NMR data (Table 1) revealed the presence of a trisubstituted furoquinoline, which was indicated by the typical adjacent protons of a furan moiety at δ_H 7.59 (1H, d, *J* = 2.7 Hz, H-2) and 7.00 (1H, d, *J* = 2.7 Hz, H-3) [23] and two aromatic singlet signals at δ_H 7.45 and 7.34. Meanwhile, two methoxys (δ_H 4.03 and 4.00), two methyls (both δ_H 1.77), an oxymethylene [δ_H 4.93 (1H, dd, *J* = 9.8, 3.7 Hz) and 4.75 (1H, dd, *J* = 9.8, 6.8 Hz)], and an oxymethine [δ_H 4.18 (1H, dd, *J* = 6.8, 3.7 Hz)] signals were also observed in the ^{1}H NMR data (Table 1). In the ^{13}C-NMR data of **1**, there were 18 carbon resonances, comprising two methyls, two methoxyls, one methylene, five methines (four olefinic and one oxygenated aliphatic), and eight quaternary carbons, which were very similar to those of (2*S*)-1-[(6,7-dimethoxyfuro[2,3-*b*]quinolin-4-yl)oxy]-3-methyl-butane-2,3-diol [24]. Considering the molecular formula of **1**, one of the two hydroxy groups of (2*S*)-1-[(6,7-dimethoxyfuro[2,3-*b*]quinolin-4-yl)oxy]-3-methyl-butane-2,3-diol was deduced to be substituted by a chlorine atom in **1**. The above deductions were further confirmed by 2D NMR experiments (Figure 2). The two methoxy groups showed HMBC cross-peaks with the carbon at δ_C 148.1 and 152.8, respectively, locating them at positions C-6 and C-7; H_2-1′ [δ_H 4.93 (dd, *J* = 9.8, 3.7 Hz) and 4.75 (dd, *J* = 9.8, 6.8 Hz)] presented an HMBC correlation to C-4 (δ_C 154.4), suggesting that the oxygenated prenyl unit was linked to C-4 of furoquinoline via an oxygen bridge. In addition, the chlorine at C-3′ and the hydroxy group at C-2′ were indicated by the key COSY correlations (Figure S11, Supporting Information) of –OH [δ_H 8.12 (1H, d, *J* = 6.2 Hz)], H-2′ [δ_H 4.58 (1H, ddd, *J* = 7.4, 6.2, 2.8 Hz)], and H-1′ [δ_H 5.35 (1H, dd, *J* = 9.6, 2.8 Hz), 5.11 (1H, dd, *J* = 9.6, 7.4 Hz)] in C_5D_5N. Thus, the planar structure of **1** was established as shown (Figure 1) and denominated as claulenine A.

Table 1. ^{1}H-NMR (500 MHz) and ^{13}C (125 MHz) NMR Data of **1**–**5** (δ in ppm).

No.	1 [a]		2 [a]		3 [a]		4 [b]		5 [a]	
	δ_H (*J* in Hz)	δ_C, Type	δ_H (*J* in Hz)	δ_C, Type	δ_H (*J* in Hz)	δ_C, Type	δ_H (*J* in Hz)	δ_C, Type	δ_H (*J* in Hz)	δ_C, Type
1				135.4, C						129.5, C
2	7.59, d (2.7)	143.0, CH	7.33, overlap	128.8, CH		160.4, C		163.6, C	7.52, br s	131.4, CH
3	7.00, d (2.7)	104.5, CH	7.45, m	128.1, CH		131.0, C	6.13, d (9.4)	112.4, CH		127.9, C
3a		103.0, C								
4		154.4, C	7.33, overlap	129.8, CH	7.47, s	138.2, CH	7.77, d (9.4)	146.2, CH		158.9, C
4a		113.2, C				113.3, C		114.3, C		
5	7.45, s	100.1, CH	7.45, m	128.1, CH	7.19, s	123.4, CH	7.33, s	125.3, CH		126.6, C
6		148.1, C	7.33, overlap	128.8, CH		124.7, C		126.7, C	7.52, br s	130.7, CH
7		152.8, C	7.64, d (15.5)	142.7, CH		162.4, C		164.7, C	9.82, s	191.4, CH
8	7.34, s	106.8, CH	6.95, d (15.5)	118.5, CH	6.70, s	97.3, CH	6.67, s	98.3, CH		
8a		142.7, C				154.8, C		156.9, C		
9		162.9, C		166.7, C						
1′	4.93, dd (9.8, 3.7)	72.5, CH_2	6.38, d (8.6)	127.1, CH		40.4, C	3.43, dd (15.9, 9.5)	34.7, CH_2	2.78, d (7.4, 3.8)	34.7, CH_2
	4.75, dd (9.8, 6.8)						3.16, overlap			
2′	4.18, dd (6.8, 3.7)	77.1, CH	6.20, d (8.6)	125.6, CH	6.16, dd (17.4, 10.7)	145.7, CH	5.47, t-like (8.7)	86.3, CH	2.68, m	46.4, CH
3′		71.9, C		127.0, C	5.08, d (10.7)	112.2, CH_2		145.6, C		146.2, C
					5.07, d (17.4)					
4′	1.77, s	29.5, CH_3	7.28, d (8.7)	130.2, CH	1.46, s	24.2, CH_3	4.44, d (12.8)	70.0, CH_2	4.78, s	112.8, CH_2
							4.19, d (12.8)		4.70, s	
5′	1.77, s	29.0, CH_3	6.83, d (8.7)	114.2, CH	1.35, s	24.2, CH_3	5.26, d (13.9)	114.1, CH_2	1.71, s	19.4, CH_3
6′	4.00, s	56.1, CH_3		159.5, C					2.44, m	32.3, CH_2
7′	4.03, s	56.2, CH_3	6.83, d (8.7)	114.2, CH					6.35, t (7.2)	153.2, CH
8′			7.28, d (8.7)	130.2, CH						139.7, C
9′			3.78, s	55.4, CH_3					9.33, s	195.4, CH
10′			3.10, s	34.6, CH_3					1.70, s	9.5, CH_3
1″					3.19, m	29.7, CH_2	4.23, d (7.8)	103.6, CH	3.43, d (7.2)	30.7, CH_2
2″					4.71, t (8.8)	91.0, CH	3.16, overlap	75.0, CH	5.30, m	120.5, CH
3″						71.8, C	3.38, m	78.0, CH		137.7, C
4″					1.46, s	26.2, CH_3	3.21, overlap	71.6, CH	1.82, s	26.0, CH_3
5″					1.22, s	24.4, CH_3	3.21, overlap	78.0, CH	1.84, s	18.2, CH_3
6″							3.81, d (11.9)	62.7, CH_2		
							3.60, dd (11.9, 4.9)			

[a] measured in $CDCl_3$. [b] measured in MeOD.

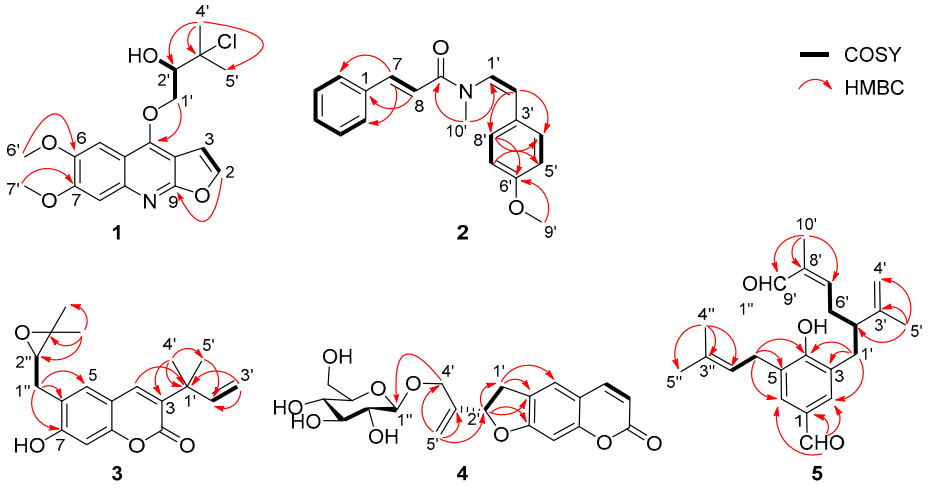

Figure 2. Key HMBC correlations of compounds **1**−**5**.

However, **1** was isolated as a raceme indicated by its zero specific rotation value and no Cotton effects in the electronic circular dichroism (ECD) spectrum. Further HPLC separation on chiral phase afforded the enantiomers of (+)-**1a** and (–)-**1b** (Figure S14, Supporting Information). To clarify their absolute configurations, ECD calculations were utilized, and the results showed that the ECD spectrum of (*R*)-**1** matched well with the experimental curve of (+)-**1a** (Figure 3). This conclusion was finally confirmed by the single-crystal X-ray diffraction for (+)-**1a** using Cu Kα radiation (Figure 4). Considering that there are fewer phytochemicals containing chlorine atoms, a freshly prepared methanol extract of the title plant was detected by using the multiple reaction monitoring (MRM) mode of UPLC/Qtrap-MS/MS, and the results suggested that **1** comes from natural source (Figure S15, Supporting Information).

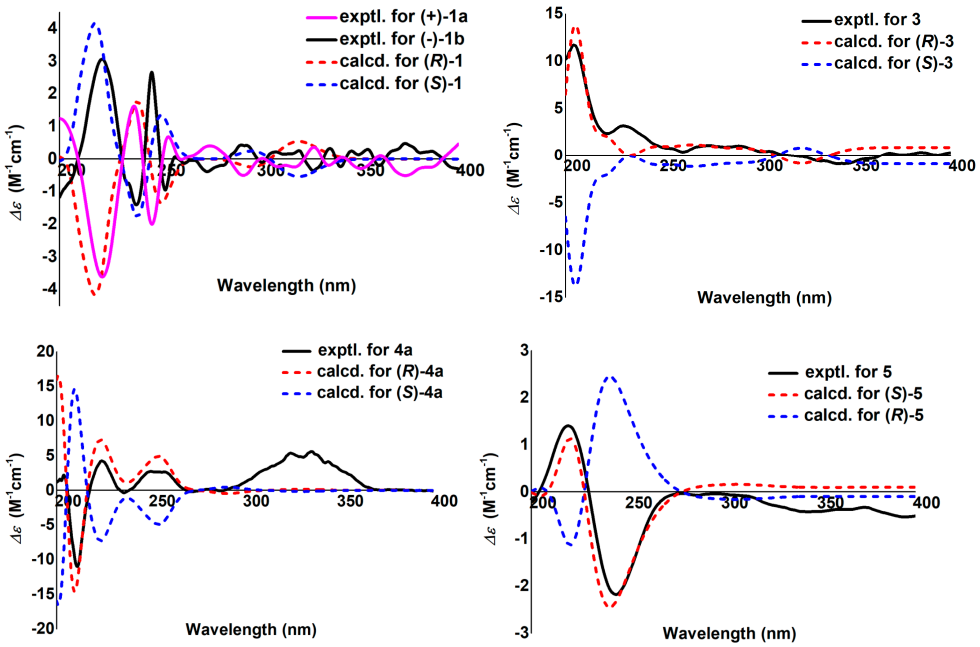

Figure 3. Experimental and calculated ECD spectra of **1**, **3**, **4a**, and **5**.

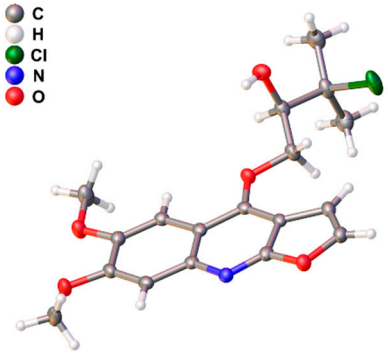

Figure 4. Plot of X-ray crystallographic data for (+)-**1a**.

Claulenine B (**2**) was obtained as a yellow oil, and its molecular formula was determined as $C_{19}H_{19}NO_2$ from the HR-ESI-MS ion at m/z 294.1490 $[M + H]^+$ (calcd for $C_{19}H_{20}NO_2$, 294.1494; mass error −1.4 ppm) and ^{13}C-NMR data. In the ^{1}H NMR spectrum, except for the up-field shifts at δ_H 3.78 (–OCH_3) and 3.10 (–NCH_3), the remaining signals were in the aromatic region (δ_H 6.2–7.7). The ^{13}C NMR data displayed 19 carbons including a signal of amide (δ_C 166.7). Careful analysis of ^{1}H and ^{13}C NMR data revealed that the signals of **2** resembled those of anhydromarmeline [25], except that the prenyl moiety was replaced by a methoxy group and an additional methyl positioned at the nitrogen atom in **2**. The HMBC correlations (Figure 2) of –OCH_3/C-6′ (δ_C 159.5) and –NCH_3/C-1′ (δ_C 127.1), C-9 (δ_C 166.7) supported the deduction. Besides, the coupling constant of olefinic protons (J = 15.5 Hz for H-7 and H-8; J = 8.6 Hz for H-1′ and H-2′) pointed out that they were *E*- and *Z*-oriented, respectively. Hence, the gross structure of claulenine B (**2**) was depicted as given (Figure 1).

Claulenin A (**3**), a yellow oil, gave a molecular formula of $C_{19}H_{22}O_4$ (nine degrees of unsaturation), as established by the $[M + H]^+$ ion at m/z 315.1594 (calcd for $C_{19}H_{23}O_4$, 315.1596; mass error −0.6 ppm) in the HR-ESI-MS. The UV spectrum appeared maximum absorptions at 335, 298, 250, and 227 nm, which is typical of the coumarin nucleus [26]. The ^{1}H NMR data of **3** (Table 1) exhibited four methyl singlets (δ_H 1.22, 1.35, 1.46, and 1.46) and three aromatic/olefinic protons [δ_H 7.47 (s), 7.19 (s), and 6.70 (s)]. The ^{13}C-NMR and HSQC spectra displayed 19 carbons classified into four methyls, two methylenes (one aliphatic

and one olefinic), five methines (one oxygenated aliphatic and four olefinic), and eight quaternary (one ester carbonyl, two aliphatic, and five olefinic, including two oxygenated) carbons. The ^{1}H and ^{13}C-NMR data of **3** bore a close resemblance to those of gravelliferone A [19], except that the methoxyl at C-7 in gravelliferone A was replaced by a hydroxy in **3**, which was supported by the molecular formula of **3** and the chemical shift of C-7 (δ_C 162.4). Therefore, the planar structure of **3** was deduced.

To clarify the absolute configuration of the only chiral center in **3**, ECD calculation was performed. The ECD experimental curve was in good agreement with the calculated one of (*R*)-**3** (Figure 3). Taken together, the structure of **3** was finally assigned and named claulenin A.

Clauleside A (**4**) exhibited an $[M - H]^-$ ion at m/z 405.1187 in the HR-ESI-MS, corresponding to a molecular formula of $C_{20}H_{22}O_9$ (calcd for $C_{20}H_{21}O_9$, 405.1186; mass error 0.2 ppm). The UV spectrum is similar to that of **3**, indicating that **4** is also a coumarin derivative. Inspection of ^{1}H-NMR and ^{13}C-NMR data (Table 1) found a set of characteristic glucosyl signals [δ_H 4.23 (1H, d, *J* = 7.8 Hz), 3.81 (1H, d, *J* = 11.9 Hz), 3.60 (1H, dd, *J* = 11.9, 4.9 Hz), 3.16–3.38 (4H, m); δ_C 103.6, 78.0, 78.0, 75.0, 71.6, 62.7], which identified **4** as a coumarin glucoside. Further analysis of NMR data of the aglycone moiety showed that they were basically consistent with those of scataccanol [27]. The HMBC correlations (Figure 2) of H_2-4′ [δ_H 4.44 (1H, d, *J* = 12.8 Hz), 4.19 (1H, d, *J* = 12.8 Hz)] to C-1″ (δ_C 103.6) deduced the linkage of the glucosyl moiety at the C-4′.

The *β*-D-glucose was demonstrated via analysis of the coupling constant (7.8 Hz) of the anomeric proton [28] and the aryl thiocarbamate derivate of the hydrolyte by HPLC (Figure S40, Supporting Information). The absolute configuration of aglycone moiety (**4a**) was assigned as (2′*R*) by comparison of the experimental and calculated ECD curves (Figure 3). Finally, **4** was established as scataccanol 4′-*O*-*β*-D-glucopyranoside and referred to as clauleside A.

Claulenin B (**5**) was isolated as a yellow oil. Its positive-ion HR-ESI-MS data at *m*/*z* 363.1933 $[M + Na]^+$ (calcd for $C_{22}H_{28}O_3Na$, 363.1936; mass error −0.8 ppm) established a molecular formula of $C_{22}H_{28}O_3$, with nine indices of hydrogen deficiency. The ^{1}H NMR data (Table 1) of **5** showed signals of two aromatic protons [δ_H 7.52 (2H, br s)] and four methyls [δ_H 1.70, 1.71, 1.82, and 1.84 (each 3H, s)]. Moreover, the ^{13}C-NMR (Table 1) and HSQC (Figure S47, Supporting Information) spectra revealed 22 carbon signals, including two aldehyde-carbonyls (δ_C 195.4 and 191.4), seven aromatic/olefinic quaternary carbons, five methines (one aliphatic and four olefinic), four methylenes (three aliphatic and one olefinic), and four methyls. The presence of three prenyl derivative units in **5** was illustrated through the HMBC correlations (Figure 2) of H_3-5′ to C-2′ (δ_C 46.4), C-3′ (δ_C 146.2), C-4′ (δ_C 112.8), H_3-10′ to C-7′ (δ_C 153.2), C-8′ (δ_C 139.7), C-9′ (δ_C 195.4), H_3-4″ to C-2″ (δ_C 120.5), C-3″ (δ_C 137.7), C-5″ (δ_C 18.2), and the COSY correlations (Figure 2) of H_2-1′/H-2′, H_2-6′/H-7′, and H_2-1″/H-2″ (δ_H 5.30). In addition, the COSY correlation of H_2-6′/H-2′ indicated that the C-6′ of one prenyl unit was connected to another prenyl unit at C-2′, forming a geranyl unit. An aldehyde group at C-9′ and a terminal double bond at C-3′ and C-4′ were further demonstrated by the HMBC correlations of –CHO (δ_H 9.33, s) to C-8′, C-10′ (δ_C 9.5) and H_2-4′ (δ_H 4.78 and 4.70, both s) to C-2′, C-5′ (δ_C 19.4). The geranyl and the prenyl units were determined to be located at the C-3 and C-5 of *p*-hydroxybenzaldehyde, respectively, from the HMBC correlations of H_2-1′ to C-2 (δ_C 131.4), C-3 (δ_C 127.9), C-4 (δ_C 158.9), H_2-1″ to C-4, C-5 (δ_C 126.6), C-6 (δ_C 130.7), and –CHO (δ_H 9.82, s) to C-1 (δ_C 129.5), C-2, C-6. In summary, the planar structure of **5** was depicted as shown (Figure 1).

The absolute configuration of C-2′ was determined by the ECD calculation. The results (Figure 3) shown that the calculated ECD spectrum of (2′*S*)-**5** agrees well with the experimental one, which allowed the absolute configuration of **5** to be specified as 2′*S*. As a result, the structure of claulenin B (**5**) was clarified.

Thirty-two known compounds were identified as 4-methoxy-*N*-methyl-2-quinolone (**6**) [29], (–)-(*S*)-edulinine (**7**) [30], dictamine (**8**) [31], pteleine (**9**) [32], cinnamamide (**10**) [33], *N*-methylcinnamamide (**11**) [34], (*Z*)-*N*-methyl-3-phenylacrylamide (**12**) [35], *N*-2-phenylethy

lcinnamamide (**13**) [36], lansiumamide A (**14**) [37], lansiumamide B (**15**) [37], (2*E*)-3-phenyl-*N*-[(*E*)-2-phenylvinyl]acrylamide (**16**) [38], lansamide I (**17**) [39], 2-benzothiazolol (**18**) [40], indole (**19**) [41], *N*,*N*′-bis[2(1*H*-indol-3-yl)ethyl]urea (**20**) [42], demethylsuberosin (**21**) [43], swietenocoumarin I (**22**) [44], xanthyletin (**23**) [45], 3′-hydroxyxanthyletn (**24**) [46], (–)-3-(*R*)-decursinol (**25**) [47], dimethyl allyl xanthyletin (**26**) [48], 3-(1,1-dimethylallyl)decursinol (**27**) [49,50], imperatorin (**28**) [51], phellopterin (**29**) [52], (–)-heraclenol (**30**) [53,54], (+)-isoangenomalin (**31**) [55], nodakenetin (**32**) [56], chalepin (**33**) [57], 6-methoxymicrominutinin (**34**) [58], marmesinin (**35**) [59], marmesin glycoside (**36**) [60], (2*R*)-2′-hydroxymarmesin (**37**) [61], and (4′-methyl-[1,1′-biphenyl]-2-yl)(*p*-tolyl)methanone (**38**) [62], by comparing their spectroscopic data with those reported in the literature. The absolute configuration of **22** was first defined as *S* by comparing the calculated and experimental ECD spectra (Figure S51, Supporting Information). In addition, **20** and **38** were reported as natural products for the first time, and **7**–**10**, **12**, **16**, **18**–**21**, **24**, **25**, **27**, **29**, **32**, and **34**–**38** and all of the isolates except **23**, **26**, **28**, **31**, and **33** were obtained for the first time from *Clausena* species and *C. lenis*, respectively.

2.2. Anti-Neuroinflammatory Activities

The 95% and 50% ethanol extract (CLT) of *C. lenis*, along with its three partitioned extracts with different polarity solvents, i.e., petroleum ether extract (CLPE), ethyl acetate extract (CLEA), and *n*-BuOH extract (CLnB) were evaluated for anti-neuroinflammatory activities based on reduction of NO production stimulated by LPS in BV-2 microglial cells. The results exhibited that NO production can be dose-dependently inhibited in the range of 10–80 μg/mL (Figure 5). To further investigate which compounds are responsible for the effect, all of these isolates (**1**–**38**) were subjected to an evaluation of their anti-neuroinflammatory activities using the same method. Six compounds (**2**, **23**, **27**, **28**, **33**, and **34**) inhibited NO production by more than 50% at 50 μM and their IC_{50} values were finally determined to be from 17.6 to 40.9 μM (Table 2). Dexamethasone (DEX) was used as a positive control. Alongside this, no cytotoxicity was observed in BV-2 microglial cells treated by these test subjects at 50 μM (cell viability > 95%).

Table 2. NO inhibition toward LPS-induced BV-2 cells.

Compound	IC_{50} (μM)
2	32.0 ± 1.4
23	40.9 ± 0.3
27	23.1 ± 0.4
28	38.1 ± 2.0
33	17.6 ± 0.6
34	19.9 ± 0.7
DEX [a]	9.6 ± 0.3

[a] Dexamethasone, as a positive control. Values are expressed as mean ± SD (n = 3).

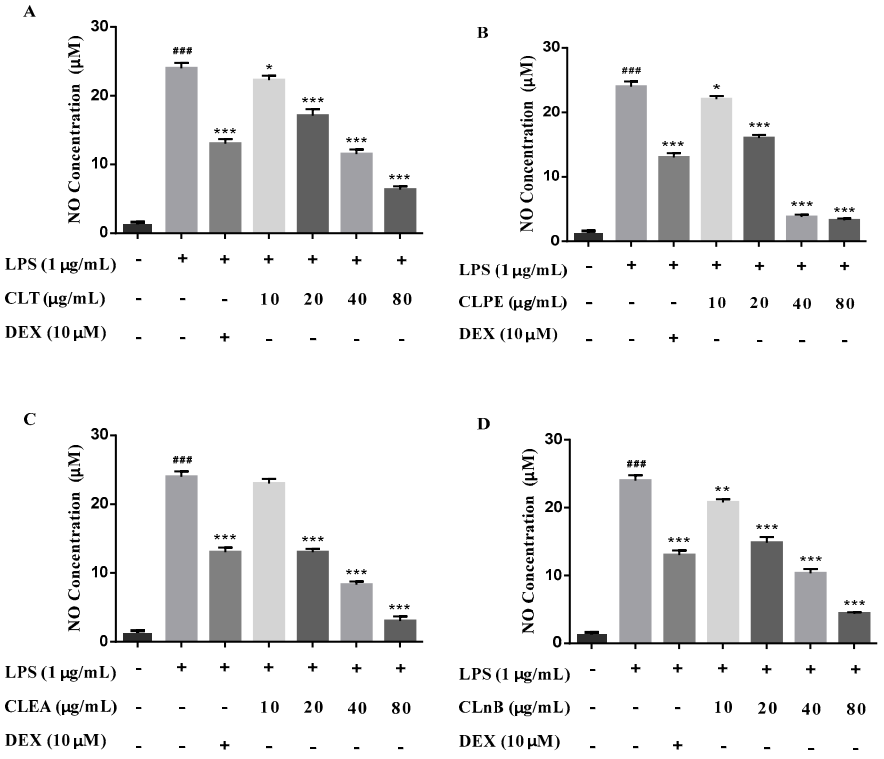

Figure 5. The production of NO stimulated by LPS in BV-2 cells. (**A**) Inhibitory effects of CLT on LPS-induced NO production in BV-2 cells. (**B**) Inhibitory effects of CLPE on LPS-induced NO production in BV-2 cells. (**C**) Inhibitory effects of CLEA on LPS-induced NO production in BV-2 cells. (**D**) Inhibitory effects of CLnB on LPS-induced NO production in BV-2 cells. Data were presented as the mean ± SD of three independent experiments. ### $p < 0.001$ *versus* control group, * $p < 0.05$, ** $p < 0.01$, *** $p < 0.001$ *versus* LPS group. (CLT: the 95% and 50% ethanol total extract of *C. lenis*; CLPE: petroleum ether extract of *C. lenis*; CLEA: ethyl acetate extract of *C. lenis*; CLnB: *n*-BuOH extract of *C. lenis*; DEX: dexamethasone, as the positive control).

2.3. Interactions of Bioactive Compounds with iNOS

Nitric oxide synthases (NOSs) catalyze the NO production using oxygen and nitrogen derived from arginine. Inducible NOS (iNOS) is one of the isoenzymes of NOSs and plays a major part in NO production during inflammation [63]. In recent years, structure-based calculations have been widely used to predict the pharmacological mechanisms of active compounds, among which molecular docking is a commonly used method [64]. To explore the possible mechanism of those bioactive compounds against NO production, we investigated the interaction between iNOS and compounds **2**, **23**, **27**, **28**, **33**, and **34** by molecular docking [65,66]. The results showed that compounds **27** and **33** had good affinities with iNOS (Glide Score < −5) (Table 3), and both of them have a hydrogen bond with the residues TYR341 of iNOS (Figure 6). Therefore, the possible mechanism of NO inhibition of **27** and **33** is through interaction with iNOS by targeting the residues in the active pocket of iNOS.

Table 3. The glide scores of bioactive compounds with iNOS.

Compound	Glide Score
27	−5.616
33	−5.228

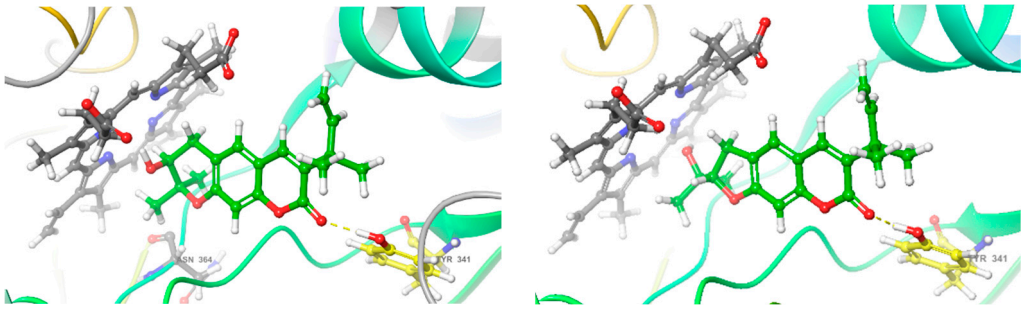

(**a**) (**b**)

Figure 6. The docking view of interaction between iNOS and compounds **27** (**a**) or **33** (**b**).

3. Discussion

Thirty-seven compounds were isolated and identified from *C. lenis* and five of them are new ones (**1**–**5**). The structures were elucidated based on MS, UV, IR, and NMR spectroscopic data and comparison with the data reported in literature. The absolute configurations of new compounds were characterized by using the ECD calculations and single-crystal X-ray diffraction analysis. (±)-Claulenine A (**1**) is a chlorine-containing furoquinoline racemate. Chlorinated natural products are rare in terrestrial plants, but common in bacteria, marine animals, and macroalgae [67,68]. **1** could be an artifact produced in the isolation procedure, but could also be generated by Fe(II)- and 2-oxoglutarate-dependent halogenases (2ODHs) [69]. The LC/MS analysis of the fresh *C. lenis* proved **1** to be originated from a natural source, but the real chlorine source is not clear. Claulenine B (**2**) is a high conjugated amide alkaloid. Claulenin A (**3**) is a prenylated coumarin with an oxirane ring and clauleside A (**4**) is a furocoumarin glucoside. Claulenin B (**5**) is a *p*-hydroxybenzaldehyde with multi-prenyl substituents. Of the known compounds, **20** and **38** are the first reported natural products, and 20 and 28 compounds are obtained from *Clausena* species and *C. lenis*, respectively, for the first time. Most of these compounds are prenylated, so the prenyltransferases play an important role in their biosyntheses.

The ethanol extract and its partitioned extracts with different polarities from *C. lenis* have significant inhibitory effects on NO production in LPS-induced BV-2 microglial cells. In the subsequent bioactivity-guided fractionation, compounds **2**, **23**, **27**, **28**, **33**, and **34** were disclosed to be the potentially active compounds with inhibition effects. Most of the bioactive compounds are coumarins, suggesting that coumarins might be the main bioactive substances for the anti-neuroinflammatory properties of the extract of *C. lenis*. Furthermore, the molecular docking results revealed that **27** and **33** had a good interaction with iNOS, which could be one of the mechanisms for their anti-inflammation effects.

4. Materials and Methods

4.1. General Experimental Procedures

Optical rotations were measured on a Rudolph Autopol IV automatic polarimeter (Rudolph Research Analytical, Hackettstown, NJ, USA). The electronic circular dichroism (ECD) and UV data were acquired on a JASCO, J-1500 CD spectrophotometer (JASCO, Tokyo, Japan). IR spectra were recorded on a Thermo Scientific Nicolet iS50 FT-IR spectrometer (Thermo Fisher Scientific, Waltham, MA, USA). HR-ESI-MS data were measured on a Waters Xevo G2 Q-TOF mass spectrometer (Waters Co., Milford, MA, USA). The nuclear magnetic resonance (NMR) spectra were obtained through a Varian INOVA-500 NMR spectrometer (Varian Co., Palo Alto, CA, USA) with TMS as an internal standard. The column chromatography (CC) was undertaken on silica gel (100−200 and 200−300 mesh, Qingdao Marine Chemical Co., Ltd., Qingdao, China), ODS-A-HG (50 μm; YMC Co., Ltd., Kyoto, Japan), and Sephadex LH-20 (Amersham Pharmacia, Uppsala, Sweden). Preparative TLC and TLC analyses were carried out on the pre-coated silica gel GF254 plates (Qingdao Marine Chemical Co., Ltd., Qingdao, China). Semi-preparative HPLC was carried out using an Agilent Eclipse XDB-C18 column (9.4 mm × 250 mm, i.d., 5 μm) on an

Agilent 1260 series LC instrument with a DAD detector (Agilent Technologies, Santa Clara, CA, USA).

4.2. Plant Material

In November 2019, dry leaves and stems of *Clausena lenis* Drake were collected from Baoting County, Hainan Province, People's Republic of China. Botanical identification was made by Prof. Pengfei Tu, one of the authors, and a voucher specimen (No. CL201911) was kept in the herbarium of Modern Research Center for Traditional Chinese Medicine, Peking University.

4.3. Extraction and Isolation

The air-dried leaves and stems of *C. lenis* (20.0 kg) were refluxed with 95% and 50% aqueous ethanol (160 L × 2 h × 2), respectively, and concentrated under reduced pressure to obtain 1.8 kg dry total extract (CLT). The extract was suspended in H_2O and extracted with petroleum ether (CLPE), ethyl acetate (CLEA), and *n*-BuOH (CLnB), successively.

The petroleum ether extract (179.1 g) was eluted by gradient elution of petroleum ether-ethyl acetate (1:0, 50:1, 30:1, 20:1, 10:1, 5:1, 3:1, 1:1, and 0:1, *v/v*) on a silica gel column to obtain 14 fractions (A−N). Fraction J (1.83 g) was subjected to Sephadex LH-20 (MeOH–CH_2Cl_2, 1:1, *v*/*v*) and produced five subfractions (J.1−J.5). Subfractions J.3 (0.70 g) and J.4 (0.27 g) were purified by semi-preparative HPLC (3.0 mL/min) to yield **2** (4.2 mg, 47% aqueous acetonitrile, t_R 29.2 min) and **9** (3.8 mg, 40% aqueous acetonitrile, t_R 15.6 min), respectively. Fraction K (14.2 g) was divided into seven fractions (K.1–K.7) by a ODS-A-HG column (aqueous MeOH, 30%–100%). Compounds **33** (26.6 mg, t_R 36.7 min) and **27** (4.5 mg, t_R 53.8 min) were obtained from subfraction K.4 (780 mg) after purification by semi-preparative HPLC (3.0 mL/min, 42% aqueous acetonitrile). Similarly, **34** (2.8 mg, t_R 16.9 min) was purified from subfraction K.2 (50 mg) by semi-preparative HPLC (3.0 mL/min, 35% aqueous acetonitrile). Fraction L (3.42 g) was fractionated into four parts (L.1–L.4) by gel filtration on Sephadex LH-20 (MeOH–CH_2Cl_2, 1:1, *v*/*v*). Subfraction L.2 (1.85 g) was subjected to an ODS-A-HG column (aqueous MeOH, 25%–100%) to give eight fractions (L.2.1–L.2.8). Subfractions L.2.1 (121.2 mg) and L.2.5 (83.4 mg) were further purified by semi-preparative HPLC (3.0 mL/min) to yield **12** (3.2 mg, 15% aqueous acetonitrile, t_R 21.8 min) and **22** (6.0 mg, 35% aqueous acetonitrile, t_R 39.9 min), respectively. Likewise, subfraction L.2.3 (131.4 mg) was purified to yield **32** (27.2 mg, 25% aqueous acetonitrile, t_R 15.7 min) and **25** (3.8 mg, 25% aqueous acetonitrile, t_R 18.4 min).

The ethyl acetate extract (160.9 g) was chromatographed on silica gel eluted with petroleum ether-ethyl acetate (1:0, 50:1, 30:1, 20:1, 10:1, 5:1, 3:1, 1:1, and 0:1, *v*/*v*) to afford 15 fractions (A−O). Fraction C (0.29 g) was fractionated on a Sephadex LH-20 column (MeOH–CH_2Cl_2, 1:1, *v*/*v*) to yield five parts (C.1–C.5). Subfraction C.3 (89.4 mg) was purified by semi-preparative HPLC (3.0 mL/min, 60% aqueous acetonitrile) to obtain **38** (1.1 mg, t_R 44.8 min) and **26** (5.1 mg, t_R 48.5 min). Fraction F (9.63 g) was divided into five parts (F.1–F.5) by an MCI GEL CHP20 column (aqueous MeOH, 50%–100%). Subfraction F.1 (129 mg) was purified by semi-preparative HPLC (3.0 mL/min, 28% aqueous acetonitrile) to yield **10** (2.7 mg, t_R 12.7 min) and **11** (17.0 mg, t_R 14.9 min). Subfraction F.3 (7.09 g) was applied to an ODS-A-HG column (aqueous MeOH, 10%–100%) and further purified by preparative HPLC (3.0 mL/min, 60% aqueous acetonitrile) to yield **14** (6.3 mg, t_R 14.4 min) and **17** (143.5 mg, t_R 21.4 min). Fraction G (7.6 g) was submitted to Sephadex LH-20 (MeOH) to acquire seven portions (G.1–G.7). Subfraction G.4 (92.3 mg) was purified by semi-preparative HPLC (50% aqueous acetonitrile, 3 mL/min) to yield **23** (2.2 mg, t_R 15.8 mind). Fraction H (4.27 g) was subjected to Sephadex LH-20 (MeOH–CH_2Cl_2, 1:1, *v*/*v*) to afford three fractions. Subfraction H.3 (130 mg) was purified by semi-preparative HPLC (3.0 mL/min, 50% aqueous acetonitrile) to yield **15** (2.0 mg, t_R 24.9 min). Fraction I (2.88 g) was separated into five fractions (I.1−I.5) using Sephadex LH-20 (MeOH). Subfraction I.3 (318 mg) was purified by semi-preparative HPLC (3.0 mL/min, 50% aqueous acetonitrile) to yield **31** (3.3 mg, t_R 13.8 min), **28** (3.4 mg, t_R 21.2 min), **29** (6.7 mg, t_R 25.2 min), and **5** (7.8 mg, t_R 50.5 min). In the same way, **8** (5.5 mg, 60%

aqueous acetonitrile, t_R 7.1 min) and **16** (6.1 mg, 60% aqueous acetonitrile, t_R 10.0 min) were obtained from subfraction I.4 (325 mg). Subfraction I.5 (0.93 g) was applied to an ODS-A-HG column (aqueous MeOH, 50%–100%) and further purified by preparative HPLC (3.0 mL/min, 25% aqueous acetonitrile) to yield **18** (8.5 mg, t_R 17.8 min). Fraction K (16.5 g) was fractionated by Sephadex LH-20 (MeOH–CH_2Cl_2, 1:1, *v*/*v*) to give five fractions. Subfraction K.3 (0.75 g) was separated into five fractions by an ODS-A-HG column (aqueous MeOH, 20%–100%). Subfraction K.3.2 (140 mg) was subjected to preparative TLC (petroleum ether-ethyl acetate, 3:1, *v*/*v*) and further purified by semi-preparative HPLC (3 mL/min, 22% aqueous acetonitrile) to afford **21** (1.9 mg, t_R = 46.2 min). Fraction L (2.86 g) was subjected to Sephadex LH-20 (MeOH–CH_2Cl_2, 1:1, *v*/*v*) to afford five fractions. Subfraction L.3 (0.56 g) and L.4 (0.30 g) was submitted to an ODS-A-HG column (aqueous MeOH, 30%–100%) to yield eight and six fractions, respectively. And subfractions L.3.4 (107.6 mg) and L.4.3 (71.3 mg) were purified by semi-preparative HPLC (3.0 mL/min) to yield **13** (3.1 mg, t_R 13.5 min, 50% aqueous acetonitrile) and **20** (0.5 mg, t_R 30.6 min, 35% aqueous acetonitrile), respectively. Fraction M (17.1 g) was applied to a silica gel column, eluting with petroleum ether-ethyl acetate (10:1, 8:1, 5:1, 3:1, and 1:1, *v*/*v*) to obtain fractions from M.1 to M.8. Subfraction M.5 (1.7 g) was subjected to Sephadex LH-20 (MeOH–CH_2Cl_2, 1:1, *v*/*v*) to afford three fractions. Subfraction M.5.2 (1.26 g) was submitted to an ODS-A-HG column (aqueous MeOH, 10%–100%) to yield three fractions. Among them, subfraction M.5.2.2 (135.1 mg) was purified by semi-preparative HPLC (3.0 mL/min, 45% aqueous acetonitrile) to yield **3** (3.8 mg, t_R 28.5 min).

The *n*-BuOH extract (222.8 g) was subjected to macroporous resin HP-20 (aqueous ethanol, 0%, 20%, 50%, 70%, and 95%) to provide five portions (A–E). Fraction C (27.3 g) was divided into nine parts (C.1–C.9) by an ODS-A-HG column (aqueous MeOH, 5%–100%). Subfraction C.4 (2.50 g) was separated into three fractions (C.4.1–C.4.3) using a Sephadex LH-20 column (MeOH–CH_2Cl_2, 1:1, *v*/*v*). Subfraction C.4.2 (1.44 g) was subjected to a silica gel column with a stepwise gradient of CH_2Cl_2–MeOH (20:1, 15:1, 10:1, 8:1, 5:1, 3:1, and 1:1) to produce nine fractions (C.4.2.1−C.4.2.9). Subfractions C.4.2.6 (210 mg) were purified by semi-preparative HPLC (3.0 mL/min) to yield **37** (2.8 mg, 15% aqueous acetonitrile, t_R 12.8 min). Subfraction C.5 (2.77 g) was separated by a Sephadex LH-20 column (MeOH–CH_2Cl_2, 1:1, *v*/*v*) to obtain three fractions (C.5.1–C.5.3). Subfraction C.5.2 (1.64 g) was further purified by a silica gel column with a gradient of CH_2Cl_2–MeOH system (20:1, 10:1, 8:1, 5:1, 1:1, and 0:1) to get **35** (9.8 mg). In addition, subfraction C.5.3 (180 mg) was further purified by preparative TLC (CH_2Cl_2–MeOH, 8:1, *v*/*v*) and semi-preparative HPLC (3.0 mL/min, 20% aqueous acetonitrile) to yield **36** (1.8 mg, t_R 27.3 min). Subfraction C.7 (2.36 g) was fractionated into four parts (C.7.1–C.7.4) by using Sephadex LH-20 (MeOH–CH_2Cl_2, 1:1, *v*/*v*). Subfraction C.7.2 (1.29 g) was eluted by gradient elution of CH_2Cl_2–MeOH (1:0, 100:1, 50:1, 20:1, 10:1, 8:1, 5:1, and 1:1, *v*/*v*) on a silica gel column to obtain nine fractions (C.7.2.1− C.7.2.9). Subfractions C.7.2.3 (13.5 mg) and C.7.2.5 (83.2 mg) were purified by semi-preparative HPLC (3.0 mL/min) to yield **24** (0.6 mg, 25% aqueous acetonitrile, t_R 23.4 min) and **7** (3.2 mg, 20% aqueous acetonitrile, t_R 37.8 min). Fraction D (30.5 g) was divided into eight parts (D.1–D.8) by an ODS-A-HG column (aqueous MeOH, 10%–100%). Subfraction D.4 (1.9 g) was fractionated into three parts (D.4.1–D.4.3) by using Sephadex LH-20 (MeOH–CH_2Cl_2, 1:1, *v*/*v*). Subfraction D.4.2 (1.03 g) was applied to a silica gel column (CH_2Cl_2–MeOH, 10:1, 5:1, 1:1, and 0:1, *v*/*v*) to produce seven subfractions (D.4.2.1−D.4.2.7). Purification of subfraction D.4.2.4 (130 mg) by semi-preparative HPLC with 16% aqueous acetonitrile (3.0 mL/min) afforded **4** (22.7 mg, t_R 22.8 min). Subfraction D.5 (2.6 g) was subjected to a Sephadex LH-20 column (MeOH–CH_2Cl_2, 1:1, *v*/*v*) to afford three fractions (D.5.1−D.5.3). Subfraction D.5.2 (1.07 g) was applied to a silica gel column, eluting with CH_2Cl_2–MeOH (100:1, 50:1, 20:1, 10:1, 5:1, 1:1, and 0:1, *v*/*v*), to give seven fractions (D5.2.1−D.5.2.7). Subfraction D.5.2.1 (90 mg) was further purified by semi-preparative HPLC (3.0 mL/min, 18% aqueous acetonitrile) to afford **30** (1.0 mg, t_R 45.4 min). Fraction E (3.3 g) was fractionated into five parts (E.1–E.5) by gel filtration on Sephadex LH-20 (MeOH–CH_2Cl_2, 1:1, *v*/*v*). Subfraction E.2 (1.72 g) was subjected to a silica gel column (petroleum ether–ethyl acetate, 5:1, 3:1, 2:1, 1:1, and 0:1, *v*/*v*) to give nine fractions

(E.2.1–E.2.9). Subfraction E.2.8 (245.1 mg) was further purified by semi-preparative HPLC (3.0 mL/min, 50% aqueous acetonitrile) to yield **6** (1.6 mg, t_R 9.0 min) and **1** (4.1 mg, t_R 17.1 min). The chiral HPLC separation of racemic **1** was performed using a Chiralpak IA column (10 × 250 mm, 5 mm, Daicel, Nanning, China), eluting with *n*-hexane-isopropanol (85:15, *v/v*). The detection wavelength was 254 nm, the column temperature was 30 °C, and the flow rate was 3 mL/min. Finally, compounds (+)-**1a** (1.9 mg, t_R 18.7 min) and (−)-**1b** (1.8 mg, t_R 22.7 min) were obtained. Subfraction E.3 (0.49 g) was subjected to a silica gel column (petroleum ether–ethyl acetate, 1:0, 50:1, 30:1, 10:1, 5:1, 3:1, and 1:1, *v/v*) to give **19** (5.5 mg).

4.3.1. (±)-Claulenine A (**1**)

White solid; $[\alpha]_D^{25}$ 0 (*c* 0.12, MeOH); UV (MeOH) λ_{max} (log ε) 337 (3.54), 321 (3.82), 309 (3.68), 247 (4.46) nm; IR (KBr) ν_{max} 2932, 1622, 1589, 1507, 1482, 1433, 1368, 1260, 1215, 1089, 1011 cm^{-1}; ^1H and ^{13}C-NMR data, see Table 1; HR-ESI-MS *m/z* 366.1101 $[M + H]^+$ (calcd for $C_{18}H_{21}NO_5Cl$, 366.1108).

(+)-Claulenine A [(+)-**1a**]: White solid, $[\alpha]_D^{25}$ + 38 (*c* 0.12, MeOH); ECD (MeOH) λ_{max} ($\Delta\varepsilon$) 246 (−2.00), 238 (+1.62), 222 (−3.61) nm.

(−)-Claulenine A [(−)-**1b**]: White solid, $[\alpha]_D^{25}$ − 42 (*c* 0.10, MeOH); ECD (MeOH) λ_{max} ($\Delta\varepsilon$) 247 (+2.44), 238 (−1.41), 223 (+2.99) nm.

4.3.2. Claulenine B (**2**)

Yellow oil; UV (MeOH) λ_{max} (log ε) 290 (3.52), 267 (3.57), 219 (3.54), 200 (3.72) nm; IR (KBr) ν_{max} 2932, 1653, 1607, 1510, 1451, 1371, 1253, 1172, 1086, 1032, 765 cm^{-1}; ^1H and ^{13}C-NMR data, see Table 1; HR-ESI-MS *m/z* 294.1490 $[M + H]^+$ (calcd for $C_{19}H_{20}NO_2$, 294.1494).

4.3.3. Claulenin A (**3**)

Yellow oil; $[\alpha]_D^{25}$ − 25 (*c* 0.24, MeOH); ECD (MeOH) λ_{max} ($\Delta\varepsilon$) 232 (+3.12), 222 (+2.37), 206 (+11.31) nm; UV (MeOH) λ_{max} (log ε) 335 (3.20), 298 (2.89), 250 (3.34), 227 (3.26), 202 (3.68) nm; IR (KBr) ν_{max} 2967, 1715, 1626, 1581, 1490, 1268, 1164, 1131, 986, 784 cm^{-1}; ^1H and ^{13}C-NMR data, see Table 1; HR-ESI-MS *m/z* 315.1594 $[M + H]^+$ (calcd for $C_{19}H_{23}O_4$, 315.1596).

4.3.4. Clauleside A (**4**)

Yellow solid; $[\alpha]_D^{25}$ + 27 (*c* 0.32, MeOH); ECD (MeOH) λ_{max} ($\Delta\varepsilon$) 336 (+10.20), 270 (+1.55), 252 (+8.75), 236 (+4.69), 229 (+9.56), 211 (−3.48) nm; UV (MeOH) λ_{max} (log ε) 334 (3.93), 250 (3.79), 226 (3.94), 206 (4.20) nm; IR (KBr) ν_{max} 3381, 2932, 2882, 1712, 1626, 1568, 1486, 1446, 1363, 1124, 1076, 1038, 823, 610 cm^{-1}; ^1H and ^{13}C-NMR data, see Table 1; HR-ESI-MS *m/z* 405.1187 $[M - H]^-$ (calcd for $C_{20}H_{21}O_9$, 405.1186).

4.3.5. Claulenin B (**5**)

Yellow oil; $[\alpha]_D^{25}$ − 10 (*c* 0.20, MeOH); ECD (MeOH) λ_{max} ($\Delta\varepsilon$) 244 (−2.18), 219 (+1.40) nm; UV (MeOH) λ_{max} (log ε) 282 (3.24), 229 (3.61), 211 (3.52) nm; IR (KBr) ν_{max} 3421, 2935, 1687, 1602, 1442, 1378, 1291, 1125, 977, 896 cm^{-1}; ^1H and ^{13}C NMR data, see Table 1; HR-ESI-MS *m/z* 363.1933 $[M + Na]^+$ (calcd for $C_{22}H_{28}O_3Na$, 363.1936).

4.3.6. (*S*)-Swietenocoumarin I (**22**)

Colorless oil; $[\alpha]_D^{25}$ + 30 (*c* 0.20, MeOH); ECD (MeOH) λ_{max} ($\Delta\varepsilon$) 226 (+5.80), 204 (−12.02) nm; ESI-MS *m/z* 347 $[M + H]^+$.

4.4. ECD Calculations of **1**, **3**, **4a**, **5**, *and* **22**

Conformation searches of **1**, **3**, **4a**, **5**, and **22** using molecular mechanics calculations were performed in Spartan 14 (Wavefunction Ind.) with MMFF force field with an energy window for acceptable conformers (ewindow) of 5 kcal/mol above the ground state. Then

the predominant conformers were optimized by using the TDDFT method at B3LYP/6-31G(d) level in Gaussian 16 [70]. The optimized conformers were used for the ECD calculations, which were performed with Gaussian 16 at B3LYP/6-31+G(d) level. The solvent effects were taken into account by the polarizable-conductor calculation model (PCM, methanol as the solvent). The SpecDis v1.71 program was used to generate ECD calculation curves [71].

*4.5. X-ray Crystallography of (+)-***1a**

The single crystals of (+)-**1a** were collected from methanol solution at room temperature. An Agilent Gemini E X-ray single-crystal diffractometer with an Oxford Cryostream cooler was used to collect the single crystal data with Cu Kα radiation at T = 174.7 K. The structure was solved with the direct method using SHELXS-97 and refined anisotropically by full-matrix least-squares on F2 using SHELXL-97. The H atoms were placed in calculated positions and refined using a riding model. The absolute configuration was determined by refinement of the Flack parameter based on resonant scattering of the light atoms.

Crystal data for (+)-**1a**: $C_{18}H_{20}ClNO_5$ (M = 365.80 g/mol), monoclinic, space group $P2_1$, size 0.19 × 0.17 × 0.02 mm^3, a = 11.1628(2) Å, b = 6.63600(10) Å, c = 11.6688(2) Å, α = 90°, β = 97.049(2)°, γ = 90°, V = 857.85(3) $Å^3$, Z = 2, T = 100.00(10) K, μ(Cu Kα) = 2.230 mm^{-1}, 3400 unique (R_{int} = 0.0736, R_{sigma} = 0.0267), which were used in all calculations. The final R_1 was 0.0384 [I > 2σ(I)] and the final wR_2 was 0.1060 (all data). Flack parameter −0.003(9). Crystallographic data for **1** have been filed with Cambridge Crystallographic Data Centre (CCDC, deposition number: CCDC 2129405). These data can be obtained free of charge from the CCDC via https://www.ccdc.cam.ac.uk/structures/ (accessed on 17 December 2021).

4.6. Absolute Configurations Determination of Sugar Moiety for **4**

Compound **4** (1.0 mg) was hydrolyzed with 2 mol/L HCl (5 mL) for 5 h at 85 °C. The reaction product was extracted three times with CH_2Cl_2. After the aqueous layer was concentrated to dryness, 2 mL anhydrous pyridine containing 2.0 mg L-cysteine methyl ester hydrochloride was added and heated at 60 °C for 1 h. Subsequently, o-tolylisothiocyanate (10 μL) was added and heated at 60 °C for 1 h. D-glucose standard (2 mg) and L-glucose standard (2 mg) were respectively reacted in the same procedure. Then, each reaction mixture was filtered by a 0.22 μm membrane and analyzed directly by an Agilent Extended C18 column (250 mm × 4.6 mm, 5 μm) on an Agilent 1260 HPLC with a gradient elution of MeCN–H_2O (5:95–30:70, *v*/*v*, 0–30 min, 1.0 mL/min) at 30 °C, and UV detection wavelength was 210 nm (Figure S40, Supporting Information). The sugar moiety of **4** was detected as D-glucose by the same t_R value with that of the D-glucose standard derivative [72].

4.7. Cell Culture

Mouse BV-2 microglial cells (Peking Union Medical College Cell Bank, Beijing, China) were cultured in Dulbecco's Modified Eagle's Medium (Macgene, Beijing, China) and supplemented with 10% fetal bovine serum (Gibico, Waltham, MA, USA), penicillin (Macgene, 100 U/mL, Beijing, China), and streptomycin (Macgene, 100 μg/mL) in a humidified incubator containing 95% air and 5% CO_2 at 37 °C.

4.8. Nitric Oxide (NO) Production Measurement and Cell Viability Assay

BV-2 cells (1 × 10^5 cells/well) were cultured in 48-well plates and stimulated with 1.0 μg/mL LPS (*Escherichia coli* 0111:B4, Sigma, St. Louis, MO, USA) with or without test extracts or compounds at 37 °C for 24 h. The production of NO was tested using a commercial assay kit (Nanjing Jiancheng Bioengineering Institute, Nanjing, Jiangsu, China), according to the manufacturer's instructions. Cell culture supernatants (160 μL) were reacted with 80 μL of the Griess reagent (1% sulfanilamide, 0.1% naphthylethylene diaminedihydrochloride, and 2% phosphoric acid) for 10 min in the dark at room temperature. The absorbance

was measured at 540 nm using a microplate reader (Tecan Trading AG, Basel, Switzerland). The experiments were performed in triplicate, and the results are presented as the mean ± SD of three independent experiments. The cell viability was evaluated according to MTT assay. Dexamethasone was used as the positive control.

4.9. Molecular Docking

The crystal structure of iNOS (PDB ID: 3E6T) was obtained from the Protein Data Bank of RCSB (Research Collaboratory for Structural Bioinformatics). Docking simulations between bioactive compounds and iNOS were performed using the Maestro software suite 2015 (Schrodinger, New York, NY, USA). The ligand molecules were drawn with Chem3D Pro 14.0 (CambridgeSoft, Waltham, MA, USA) and optimized by the Ligprep module of Maestro. The protein receptor was prepared by deleting the ligand and water molecules and then was adopted for molecular docking with ligands. The reported inhibitor binding sites of iNOS was chosen as the binding pocket [73].

Supplementary Materials: The following supporting information can be downloaded at: https://www.mdpi.com/article/10.3390/molecules27061971/s1. HR-ESI-MS, UV, IR, 1D and 2D NMR spectra of **1**−**5**. Chiral HPLC separation of racemic **1**. LC/MS chromatograms of detection of **1** in the crude extract of *C. lenis*. HPLC-UV chromatograms of the derivatives of D-glucose, L-glucose, and the hydrolysate of **4**. Structures of **6**−**38**. ESI-MS and experimental and calculated ECD spectra of **22**. These materials are available online.

Author Contributions: Conceptualization, K.-W.Z., P.-F.T. and Y.J.; methodology, S.-S.Z. and Y.J.; validation, S.-S.Z., Y.-F.Z. and M.D.; investigation, S.-S.Z.; writing, review, and editing, S.-S.Z. and Y.J.; supervision, project administration and funding acquisition, Y.J. All authors have read and agreed to the published version of the manuscript.

Funding: This work was financially supported by National Natural Science Foundation of China (NSFC; Nos. 81973199, 81473106, and 81773864).

Institutional Review Board Statement: Not applicable.

Informed Consent Statement: Not applicable.

Data Availability Statement: Not applicable.

Conflicts of Interest: The authors declare no conflict of interest.

Sample Availability: Samples of the compounds are not available from the authors.

References

1. Leng, F.; Edison, P. Neuroinflammation and microglial activation in Alzheimer disease: Where do we go from here. *Nat. Rev. Neurol.* **2021**, *17*, 157–172. [CrossRef] [PubMed]
2. Rasheed, M.; Liang, J.; Wang, C.; Deng, Y.; Chen, Z. Epigenetic regulation of neuroinflammation in Parkinson's disease. *Int. J. Mol. Sci.* **2021**, *22*, 4956. [CrossRef] [PubMed]
3. Yao, L.; Wu, J.; Koc, S.; Lu, G. Genetic imaging of neuroinflammation in Parkinson's disease: Recent advancements. *Front. Cell Dev. Biol.* **2021**, *9*, 655819. [CrossRef] [PubMed]
4. DiSabato, D.J.; Quan, N.; Godbout, J.P. Neuroinflammation: The devil is in the details. *J. Neurochem.* **2016**, *139*, 136–153. [CrossRef] [PubMed]
5. Shields, D.C.; Haque, A.; Banik, N.L. Neuroinflammatory responses of microglia in central nervous system trauma. *J. Cereb. Blood Flow Metab.* **2020**, *40*, S25–S33. [CrossRef] [PubMed]
6. Shin, S.A.; Joo, B.J.; Lee, J.S.; Ryu, G.; Han, M.; Kim, W.Y.; Park, H.H.; Lee, J.H.; Lee, C.S. Phytochemicals as anti-inflammatory agents in animal models of prevalent inflammatory diseases. *Molecules* **2020**, *25*, 5932. [CrossRef] [PubMed]
7. Borah, A.; Paul, R.; Mazumder, M.K.; Bhattacharjee, N. Contribution of β-phenethylamine, a component of chocolate and wine, to dopaminergic neurodegeneration: Implications for the pathogenesis of Parkinson's disease. *Neurosci. Bull.* **2013**, *29*, 655–660. [CrossRef]
8. Kim, C.; Kim, B. Anti-cancer natural products and their bioactive compounds inducing ER stress-mediated apoptosis: A review. *Nutrients* **2018**, *10*, 1021. [CrossRef] [PubMed]
9. Rathaur, P.; SR, K.J. Metabolism and pharmacokinetics of phytochemicals in the human body. *Curr. Drug Metab.* **2020**, *20*, 1085–1102. [CrossRef] [PubMed]

10. Xia, H.M.; Li, C.J.; Yang, J.Z.; Ma, J.; Chen, X.G.; Zhang, D.; Li, L.; Zhang, D.M. A,D-seco-Limonoids from the stems of *Clausena emarginata*. *J. Nat. Prod.* **2014**, *77*, 784–791. [CrossRef] [PubMed]
11. Xia, H.M.; Li, C.J.; Yang, J.Z.; Ma, J.; Li, L.; Zhang, D.; Bao, X.Q.; Zhang, D.M. Anti-inflammatory amide alkaloids from the stems of *Clausena emarginata*. *J. Asian Nat. Prod. Res.* **2014**, *16*, 971–975. [CrossRef] [PubMed]
12. Liu, J.; Li, C.J.; Ni, L.; Yang, J.Z.; Li, L.; Zang, C.X.; Bao, X.Q.; Zhang, D.; Zhang, D.M. Anti-inflammatory alkaloid glycoside and quinoline alkaloid derivates from the stems of *Clausena lansium*. *RSC Adv.* **2015**, *5*, 80553. [CrossRef]
13. Editorial Committee of Flora of China. *Flora of China*; Science Press: Beijing, China, 1997; Volume 43, p. 138.
14. He, H.P.; Chen, S.T.; Shen, Y.M.; Chen, C.X.; Zhao, Y.B.; Hao, X.J. A novel dimeric coumarin from *Clausena lenis*. *Chin. Chem. Lett.* **2003**, *14*, 1150–1153.
15. He, H.P.; Shen, Y.M.; Chen, S.T.; He, Y.N.; Hao, X.J. Dimeric coumarin and phenylpropanoids from *Clausena lenis*. *Helv. Chim. Acta* **2006**, *89*, 2836–2840. [CrossRef]
16. Liu, Y.P.; Wen, Q.; Hu, S.; Ma, Y.L.; Jiang, Z.H.; Tang, J.Y.; Fu, Y.H.; Qiu, S.X. Furanocoumarins with potential antiproliferative activities from *Clausena lenis*. *Nat. Prod. Res.* **2019**, *33*, 2631–2637. [CrossRef] [PubMed]
17. Liu, Y.P.; Yan, G.; Xie, Y.T.; Lin, T.C.; Zhang, W.; Li, J.; Wu, Y.J.; Zhou, J.Y.; Fu, Y.H. Bioactive prenylated coumarins as potential anti-inflammatory and anti-HIV agents from *Clausena lenis*. *Bioorg. Chem.* **2020**, *97*, 103699. [CrossRef] [PubMed]
18. Yan, G.; Li, Y.J.; Zhao, Y.Y.; Guo, J.M.; Zhang, W.H.; Zhang, M.M.; Fu, Y.H.; Liu, Y.P. Neuroprotective carbazole alkaloids from the stems and leaves of *Clausena lenis*. *Nat. Prod. Res.* **2021**, *35*, 2002–2009. [CrossRef]
19. Wongthet, N.; Sanevas, N.; Schinnerl, J.; Brecker, L.; Santimaleeworagun, W.; Rosenau, T.; Bacher, M.; Vajrodaya, S. Chemical constituents of *Clausena lenis*. *Nat. Prod. Res.* **2021**, *35*, 3873–3879. [CrossRef]
20. Cao, N.K.; Chen, Y.M.; Ma, X.L.; Zeng, K.W.; Zhao, M.B.; Tu, P.F.; Li, J.; Jiang, Y. Bioactive carbazole and quinoline alkaloids from *Clausena dunniana*. *Phytochemistry* **2018**, *151*, 1–8. [CrossRef] [PubMed]
21. Cao, N.K.; Zhu, S.S.; Li, J.; Tu, P.F.; Jiang, Y. Coumarins from the stems and leaves of *Clausena dunniana* H. Lév. *Biochem. Syst. Ecol.* **2020**, *90*, 104048. [CrossRef]
22. Cao, N.K.; Zhu, S.S.; Chen, Y.M.; Ma, X.L.; Zhao, M.B.; Li, J.; Tu, P.F.; Jiang, Y. A new prenylated coumarin diglycoside with insulin-release promoting activity from *Clausena dunniana*. *J. Asian Nat. Prod. Res.* **2021**, *23*, 385–391. [CrossRef] [PubMed]
23. Ulubelen, A. Alkaloids from *Haplophyllum buxbaumii*. *Phytochemistry* **1985**, *24*, 372–374. [CrossRef]
24. He, H.P.; Shen, Y.M.; Zuo, G.Y.; Yang, X.S.; Hao, X.J. Dinorditerpene, diterpenes, alkaloids, and coumarins from *Clausena dunniana*. *Helv. Chim. Acta* **2003**, *86*, 3187–3193. [CrossRef]
25. Phuwapraisirisan, P.; Puksasook, T.; Jong-aramruang, J.; Kokpol, U. Phenylethyl cinnamides: A new series of *a*-glucosidase inhibitors from the leaves of *Aegle marmelos*. *Bioorg. Med. Chem. Lett.* **2008**, *18*, 4956–4958. [CrossRef] [PubMed]
26. Ito, C.; Fujiwara, K.; Kajita, M.; Ju-Ichi, M.; Takemura, Y.; Suzuki, Y.; Tanaka, K.; Omura, M.; Furukawa, H. New coumarins from *Citrus* plants. *Chem. Pharm. Bull.* **1991**, *39*, 2509–2513. [CrossRef]
27. Suthiwonga, J.; Thongsriband, Y.; Yenjai, C. A new furanocoumarin from the fruits of *Scaevola taccada* and antifungal activity against *Pythium insidiosum*. *Nat. Prod. Res.* **2017**, *31*, 453–459. [CrossRef]
28. Chang, H.T.; Okada, T.; Okuyama, T.; Tu, P.F. ^{1}H and ^{13}C NMR assignments for two new angular furanocoumarin glycosides from *Peucedanum praeruptorum*. *Magn. Reson. Chem.* **2007**, *45*, 611–614. [CrossRef] [PubMed]
29. Min, Y.D.; Kwon, H.C.; Yang, M.C.; Lee, K.H.; Choi, S.U.; Lee, K.R. Isolation of limonoids and alkaloids from *Phellodendron amurense* and their multidrug resistance (MDR) reversal activity. *Arch. Pharm. Res.* **2007**, *30*, 58–63. [CrossRef] [PubMed]
30. Boyd, D.R.; Sharma, N.D.; Barr, S.A.; Carroll, J.G.; Mackerracher, D.; Malone, J.F. Synthesis and absolute stereochemistry assignment of enantiopure dihydrofuro- and dihydropyrano-quinoline alkaloids. *J. Chem. Soc. Perkin Trans.* **2000**, *1*, 3397–3405. [CrossRef]
31. Sriphana, U.; Thongsri, Y.; Prariyachatigul, C.; Pakawatchai, C.; Yenjai, C. Clauraila E from the roots of *Clausena harmandiana* and antifungal activity against *Pythium insidiosum*. *Arch. Pharm. Res.* **2013**, *36*, 1078–1083. [CrossRef] [PubMed]
32. Pusset, J.; Lopez, J.L.; Pais, M.; Neirabeyeh, M.A.; Veillon, J.M. Isolation and 2D NMR studies of alkaloids from *Comptonella sessilfoliola*. *Planta Med.* **1991**, *57*, 153–155. [CrossRef] [PubMed]
33. Gómez-Calvario, V.; Rios, M.Y. ^{1}H and ^{13}C NMR data, occurrence, biosynthesis, and biological activity of Piper amides. *Magn. Reson. Chem.* **2019**, *57*, 994–1070. [CrossRef] [PubMed]
34. Shen, W.W.; Li, W.; Wang, G.C.; Wu, X.; Ye, W.C.; Li, Y.L. Chemical constituents of *Clausena lansium*. *J. Jinan Univ. (Nat. Sci.)* **2012**, *33*, 506–509.
35. Ottenbacher, R.V.; Kurganskiy, V.I.; Talsi, E.P.; Bryliakov, K.P. Manganese catalyzed enantioselective epoxidation of α,β-unsaturated amides with H_2O_2. *Adv. Synth. Catal.* **2021**, *363*, 2778–2782. [CrossRef]
36. Borges-del-Castillo, J.; Vazquez-Bueno, P.; Secundino-Lucas, M.; Martinez-Martir, A.I.; Joseph-Nathan, P. The *N*-2-phenylethylcinnamamide from *Spilanthes ocymifolia*. *Phytochemistry* **1984**, *23*, 2671–2672. [CrossRef]
37. Xu, H.Y.; Chen, T.; Huang, L.B.; Shen, Q.J.; Lian, Z.W.; Shi, Y.; Ouyang, M.A.; Song, L.Y. Synthesis and fungicidal activity of lansiumamide A and B and their derivatives. *Molecules* **2018**, *23*, 1499. [CrossRef] [PubMed]
38. Bayer, A.; Maier, M.E. Synthesis of enamides from aldenydes and amides. *Tetrahedron* **2004**, *60*, 6665–6677. [CrossRef]
39. Goossen, L.J.; Blanchot, M.; Arndt, M.; Salih, K.S.M. Synthesis of botryllamides and lansiumamides via ruthenium-catalyzed hydroamidation of alkynes. *Synlett* **2010**, *11*, 1685–1687. [CrossRef]

40. Zhou, Y.; Liu, X.Y.; Yu, H.B.; Lu, X.L.; Jiao, B.H. Research of the secondary metabolites from Antarctic-derived fungus Penicillium sp. S-2-10. *Chin. J. Mar. Drugs* **2017**, *36*, 18–22.
41. Devi, P.; Wahidullah, S.; Rodrigues, C.; Souza, L.D. The sponge-associated bacterium *Bacillus licheniformis* SAB1: A source of antimicrobial compounds. *Mar. Drugs* **2010**, *8*, 1203–1212. [CrossRef] [PubMed]
42. Bigi, F.; Frullanti, B.; Maggi, R.; Sartori, G.; Zambonin, E. Reaction of aliphatic amines with acetoacetanilide in the presence of zeolite catalyst. Solvent-free synthesis of symmetric *N*,*N*′-dialkylureas. *J. Org. Chem.* **1999**, *64*, 1004–1006. [CrossRef] [PubMed]
43. Patre, R.E.; Shet, J.B.; Parameswaran, P.S.; Tilve, S.G. Cascade Wittig reaction-double Claisen and Cope rearrangements: One-pot synthesis of diprenylated coumarins gravelliferone, balsamiferone, and 6,8-diprenylumbelliferone. *Tetrahedron Lett.* **2009**, *50*, 6488–6490. [CrossRef]
44. Rao, A.V.R.; Bhide, K.S.; Mujumdar, R.B. Phenolics from the bark of *Chloroxylon swietenia* DC.: Part II. Isolation of swietenocoumarins G, H and I. *Indian J. Chem.* **1980**, *19B*, 1046–1048.
45. Xiong, Y.T.; Huang, G.; Yao, Z.L.; Zhao, C.; Zhu, X.; Wu, Q.L.; Zhou, X.D.; Li, J.K. Screening effective antifungal substances from the bark and leaves of *Zanthoxylum avicennae* by the bioactivity-guided isolation method. *Molecules* **2019**, *24*, 4207. [CrossRef]
46. Park, H.Y.; Kwon, S.B.; Heo, N.K.; Chun, W.J.; Kim, M.J.; Kwon, Y.S. Constituents of the stem of *Angelica gigas* with Rat lens aldose reductase inhibitory activity. *J. Korean Soc. Appl. Biol. Chem.* **2011**, *54*, 194–199. [CrossRef]
47. Malikov, V.M.; Saidkhodzhaev, A.I. Coumarins. Plants, structure, properties. *Chem. Nat. Compd.* **1998**, *34*, 345–409. [CrossRef]
48. Carmo, G.D.; Fernandes, T.S.; Pedroso, M.; Ferraz, A.; Neto, A.T.; Silva, U.F.; Mostardeiro, M.A.; Back, D.F.; Dalcol, I.I.; Morel, A.F. Phytochemical and antimicrobial study of *Pilocarpus pennatifolius* Lemaire. *Fitoterapia* **2018**, *131*, 1–8. [CrossRef]
49. Macias, F.A.; Massanet, G.M.; Rodriguez-Luis, F.; Salva, J. Carbon-13 NMR of coumarins I: 3-(1,1-dimethylallyl) derivatives. *Magn. Reson. Chem.* **1989**, *27*, 705–707. [CrossRef]
50. De Moura, N.F.; Simionatto, E.; Porto, C.; Hoelzel, S.C.S.; Dessoy, E.C.S.; Zanatta, N.; Morel, A.F. Quinoline alkaloids, coumarins, and volatile constituents of *Helietta longifoliata*. *Planta Med.* **2002**, *68*, 631–634. [CrossRef] [PubMed]
51. Wang, X.B.; Li, G.H.; Li, L.; Zheng, L.J.; Huang, R.; Zhang, K.Q. Nematicidal coumarins from *Heracleum candicans* Wall. *Nat. Prod. Res.* **2008**, *22*, 666–671. [CrossRef] [PubMed]
52. Bergendorff, O.; Dekermendjian, K.; Nielsen, M.; Shan, R.; Witt, R.; Ai, J.; Sterner, O. Furanocoumarins with affinity to brain benzodiazepine receptors in vitro. *Phytochemistry* **1997**, *44*, 1121–1124. [CrossRef]
53. Kviesis, J.; Kļimenkovs, I.; Arbidans, L.; Podjava, A.; Kļaviņš, M.; Liepiņš, E. Evaluation of furanocoumarins from seeds of the wild parsnip (*Pastinaca sativa* L. *s.l.*). *J. Chromatogr. B* **2019**, *1105*, 54–66. [CrossRef] [PubMed]
54. Gowri, P.M.; Haribabu, K.; Kishore, H.; Manjusha, O.; Biswas, S.; Murty, U.S.N. Microbial transformation of (+)-heraclenin by *Aspergillus niger* and evaluation of its antiplasmodial and antimicrobial activities. *Curr. Sci.* **2011**, *100*, 1706–1711.
55. Yamaguchi, S.; Muro, S.; Kobayashi, M.; Miyazawa, M.; Hirai, Y. Absolute structures of some naturally occurring isopropenyldihydrobenzofurans, remirol, remiridiol, angenomalin, and isoangenomalin. *J. Org. Chem.* **2003**, *68*, 6274–6278. [CrossRef]
56. Saeed, M.A.; Sabir, A.W. Irritant and cytotoxic coumarins from *Angelica glauca* Edgew roots. *J. Asian Nat. Prod. Res.* **2008**, *10*, 49–58. [CrossRef] [PubMed]
57. Oliveira, F.M.; Sant'ana, A.E.G.; Conserva, L.M.; Maia, J.G.S.; Guilhon, G.M.P. Alkaloids and coumarins from *Esenbeckia* species. *Phytochemistry* **1996**, *41*, 647–649. [CrossRef]
58. Kamperdick, C.; Phuong, N.M.; Sung, T.V.; Schmidt, J.; Adama, G. Coumarins and dihydrocinnamic acid derivatives from *Micromelum falcatum*. *Phytochemistry* **1999**, *52*, 1671–1676. [CrossRef]
59. Liu, J.H.; Xu, S.X.; Meng, Z.Y.; Yao, X.S.; Wu, Y.Q. Further isolation of coumarin from *Angelica pubescence* Maxim *f. biserrata* Shan et Yuan. *J. Chin. Pharm. Sci.* **1997**, *6*, 221–224.
60. Kassim, N.K.; Lim, P.C.; Ismail, A.; Awang, K. Isolation of antioxidative compounds from *Micromelum minutum* guided by preparative thin layer chromatography-2,2-diphenyl-1-picrylhydrazyl (PTLC-DPPH) bioautography method. *Food Chem.* **2019**, *272*, 185–191. [CrossRef]
61. Lemmich, J. Monoterpene, chromone and coumarin glucosides of *Diplolophium buchananii*. *Phytochemistry* **1995**, *38*, 427–432. [CrossRef]
62. Zhang, F.M.; Shi, Z.Z.; Chen, F.; Yuan, Y. An efficient $MnCl_2$-catalyzed tandem acylation-cross-coupling reaction of o-halobenzoyl chloride with diorganyl magnesium compounds. *Appl. Organometal. Chem.* **2010**, *24*, 57–63. [CrossRef]
63. Cinelli, M.A.; Do, H.T.; Miley, G.P.; Silverman, R.B. Inducible nitric oxide synthase: Regulation, structure, and inhibition. *Med. Res. Rev.* **2020**, *40*, 158–189. [CrossRef]
64. Tasleem, M.; Alrehaily, A.; Almeleebia, T.M.; Alshahrani, M.Y.; Ahmad, I.; Asiri, M.; Alabdallah, N.M.; Saeed, M. Investigation of antidepressant properties of yohimbine by employing structure-based computational assessments. *Curr. Issues Mol. Biol.* **2021**, *43*, 1805–1827. [CrossRef] [PubMed]
65. Zhang, Y.; Liu, J.Z.; Wang, M.Y.; Sun, C.J.; Li, X.B. Five new compounds from *Hosta plantaginea* flowers and their anti-inflammatory activities. *Bioorg. Chem.* **2020**, *95*, 103494. [CrossRef] [PubMed]
66. Liang, H.; Shi, Y.; Zeng, K.; Zhao, M.; Tu, P.; Jiang, Y. Coumarin derivatives from the leaves and twigs of *Murraya exotica* L. and their anti-inflammatory activities. *Phytochemistry* **2020**, *177*, 112416. [CrossRef] [PubMed]
67. Chung, W.J.; Vanderwal, C.D. Stereoselective halogenation in natural product synthesis. *Angew. Chem. Int. Ed.* **2016**, *55*, 4396–4434. [CrossRef]

68. Li, C.; Shi, D. Structural and bioactive studies of halogenated constituents from sponges. *Curr. Med. Chem.* **2020**, *27*, 2335–2360. [CrossRef] [PubMed]
69. Kim, C.Y.; Mitchell, A.J.; Glinkerman, C.M.; Li, F.S.; Pluskal, T.; Weng, J.K. The chloroalkaloid (−)-acutumine is biosynthesized via a Fe(II)- and 2-oxoglutarate-dependent halogenase in Menispermaceae plants. *Nat. Commun.* **2020**, *11*, 1867. [CrossRef]
70. Bruhn, T.; Schaumlöffel, A.; Hemberger, Y.; Pecitelli, G. *SpecDis*, Version 1.71; Berlin, Germany, 2017. Available online: https://specdis-software.jimdo.com (accessed on 24 February 2020).
71. Frisch, M.J.; Trucks, G.W.; Schlegel, H.B.; Scuseria, G.E.; Robb, M.A.; Cheeseman, J.R.; Scalmani, G.; Barone, V.; Petersson, G.A.; Nakatsuji, H.; et al. *Gaussian 16*; Revision C.01; Gaussian, Inc.: Wallingford, CT, USA, 2016.
72. Tanaka, T.; Nakashima, T.; Ueda, T.; Tomii, K.; Kouno, I. Facile discrimination of aldose enantiomers by reversed-phase HPLC. *Chem. Pharm. Bull.* **2007**, *55*, 899–901. [CrossRef]
73. Garcin, E.D.; Arvai, A.S.; Rosenfeld, R.J.; Kroeger, M.D.; Crane, B.R.; Andersson, G.; Andrews, G.; Hamley, P.J.; Mallinder, P.R.; Nicholls, D.J.; et al. Anchored plasticity opens doors for selective inhibitor design in nitric oxide synthase. *Nat. Chem. Biol.* **2008**, *4*, 700–707. [CrossRef]